

DETECTION OF OPTICAL SYNCHROTRON EMISSION FROM THE RADIO JET OF 3C 279

C. C. CHEUNG

Department of Physics, MS 057, Brandeis University, Waltham, MA 02454

ccheung@brandeis.edu

ApJL, accepted

ABSTRACT

We report the detection of optical and ultraviolet emission from the kiloparsec scale jet of the well-known quasar 3C 279. A bright knot, discovered in archival V and U band *Hubble Space Telescope* Faint Object Camera images, is coincident with a peak in the radio jet $\sim 0.6''$ from the nucleus. The detection was also confirmed in Wide Field Planetary Camera-2 images. Archival Very Large Array and MERLIN radio data are also analyzed which help to show that the high-energy optical/UV continuum, and spectrum, are consistent with a synchrotron origin from the same population of relativistic electrons responsible for the radio emission.

Subject headings: Galaxies: active — galaxies: jets — quasars: general — quasars: individual (3C 279) — radio continuum: galaxies

1. INTRODUCTION

The quasar 3C 279 ($z=0.536$) is one of the best studied active galaxies in the sky. It is a bright EGRET γ -ray source (Hartman et al. 2001), and shows rapid variability across the entire electromagnetic spectrum (e.g., Wehrle et al. 1998). One of the first early triumphs of the technique of Very Long Baseline Interferometry (VLBI), was the discovery of apparent superluminal motion in the parsec-scale jet of this quasar (Cotton et al. 1979, and references therein). Subsequent superluminal ejections have been continually monitored for more than thirty years (e.g., Unwin et al. 1989; Wehrle et al. 2001). The VLBI jet's polarization structure (Leppänen, Zensus, & Diamond 1995) has been imaged at frequencies as high as 86 GHz (Attridge 2001). Circular polarization has been detected in the parsec-scale jet, possibly implying an electron-positron composition (Wardle et al. 1998; Homan & Wardle 1999).

The radio jet has long been known to extend out to kiloparsec scales for $\sim 5''$ to the south-southwest (de Pater & Perley 1983; Akujor et al. 1994). An extended feature to the northwest can be attributed to a radio lobe fueled by the Doppler dimmed counter-jet, but is equally likely to be due to the main jet because of its extreme viewing angle to our line of sight (Figure 1; de Pater & Perley 1983). The recent discovery of an X-ray counterpart to the $5''$ long radio jet in a deep *Chandra* exposure prompted an analysis of archival *Hubble Space Telescope*¹ (*HST*) images in search of optical emission in the jet. The *Chandra* results will be presented elsewhere (Marshall et al. 2002b). In this *Letter*, we report the detection of optical and ultraviolet (UV) emission associated with the brightest region in the kiloparsec scale radio jet. We adopt a Friedmann cosmology with $H_0 = 75 \text{ km s}^{-1} \text{ Mpc}^{-1}$ and $q_0 = 0$ throughout this *Letter*, so at the distance of the quasar, 1 arcsecond equals 5.58 kpc.

2. DESCRIPTION OF ARCHIVAL OBSERVATIONS

We obtained post-COSTAR Faint Object Camera (FOC) f/96 (Jedrzejewski et al. 1994) images of 3C 279 from the *HST* archive with ‘on-the-fly’ pipeline calibration applied. Single high quality exposures with the F253M and F550M filters (each

~ 1 ksec) were taken consecutively during November 1995 as part of a program (ID 6057) to study the inner structure of the quasar (Hook, Schreier, & Miley 2000) with the Fine Guidance Sensors (FGS) – see Table 1. These filters approximate the standard U and V bands, respectively. To our knowledge, only the FGS data have been published (E. Schreier, personal communication).

A visual inspection of the FOC images shows a noticeable linear extension centered $\sim 0.6''$ from the quasar nucleus, at a position angle (in the sky) of $\sim 205^\circ$ in both the U and V band exposures. This feature matches the position of the bright knot ‘D’ in the radio jet (nomenclature of de Pater & Perley 1983). An overlay of the optical image with a high resolution radio image (Figure 1) show that the optical feature is clearly coincident with this region of the radio jet.

We were able to confirm this detection in two short (300 sec) R-band WFPC2 F702W exposures taken more than a year apart as part of the *HST* 3CR snapshot survey (Lehnert et al. 1999). Both images unfortunately suffered from saturated nuclei, and even worse, a diffraction spike lies at the position angle of the radio jet for almost its entire $5''$ extent. However, subtracting a smoothed version of the PSF from both the individual exposures, and from the combined image, revealed a large excess above the diffraction spike at the position of knot D in each case (Figure 2). Its count rate (measured from the unsharp masked image) is about three times greater than that measured anywhere else on that or the other three diffraction spikes. We use these data only for confirming the optical identification of knot D, as any flux measurement from these images will be hopelessly contaminated.

Two more *HST* images were available in the archive at the time of our analysis from the same FOC/FGS program described above (Hook, Schreier, & Miley 2000). The observing sequence from the original program was repeated ~ 1.5 years later (on 30 May 1997), but utilized the F2ND neutral density filters in parallel which resulted in a factor of about six drop in sensitivity. Our extraction procedure was performed on the images from the later epoch and showed flux levels at the predicted position of the $0.6''$ knot to be consistent with

¹ Based on observations made with the NASA/ESA Hubble Space Telescope, obtained from the data archive at the Space Telescope Science Institute. STScI is operated by the Association of Universities for Research in Astronomy, Inc. under NASA contract NAS 5-26555.

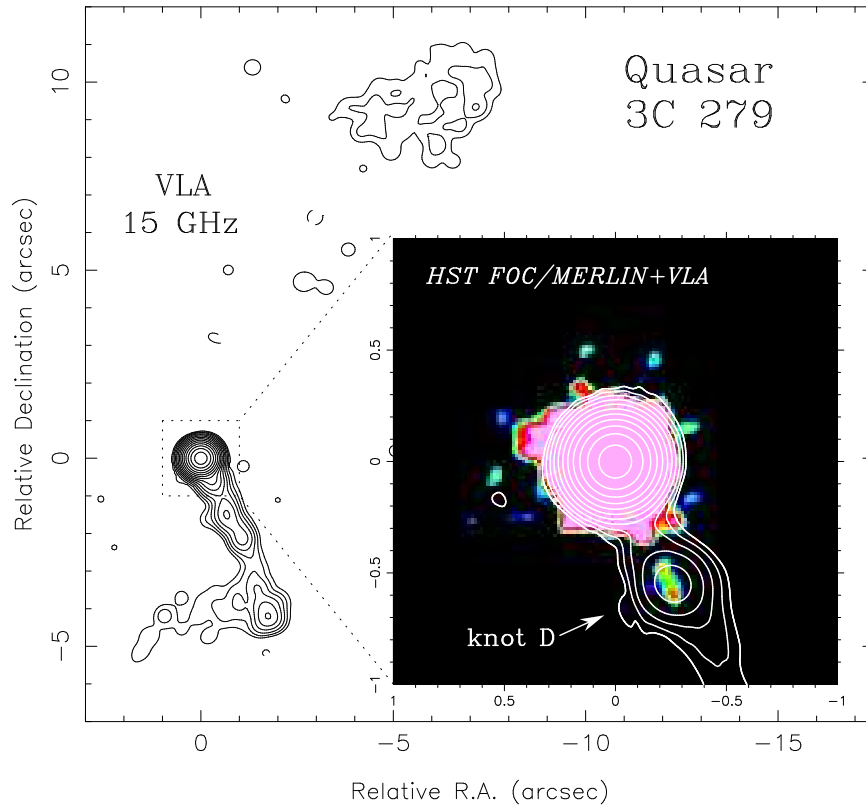


FIG. 1.— VLA 15 GHz image (resolution $0.4''$) showing the large-scale radio jet of 3C 279 at a position angle of $\sim 205^\circ$, and a radio lobe extending to the NW $\sim 10''$ away. The inset is a zoomed in view of the inner $2'' \times 2''$ field around the nucleus. The *HST* FOC V-band image (colorscale) was smoothed to a resultant resolution of about $0.08''$ and is shown with a high resolution ($0.2''$) MERLIN+VLA 5 GHz image overlaid (see Figure 2 for the full radio image and description). The images were aligned on the peaks of the nucleus. There is a clear correspondence of an optical feature with a peak in the radio jet emission at $0.6''$ (knot D – naming convention from de Pater & Perley 1983). The 15 GHz fluxes are plotted logarithmically in steps of factor 2 beginning at 1.05 mJy/beam.

the background (see §3). Fluxes for the quasar nucleus could still be extracted from these images yielding 1.1 and 3.5 mJy at U and V bands, which are consistent with contemporaneous ground-based measurements (Wehrle et al. 1998). We similarly extracted nuclear fluxes for the 1995 epoch and obtained 0.79 mJy (U) and 2.8 mJy (V), again, close to ground-based results by Hartman et al. (2001).

Radio data was obtained from the NRAO² Very Large Array (Thompson et al. 1980) archive and the MERLIN³ archive (see Table 1 for a summary). The VLA data (5 and 15 GHz) was calibrated in AIPS (Greisen 1988) utilizing standard procedures and self-calibrated in the Caltech DIFMAP package (Shepherd, Pearson, & Taylor 1994). We selected the data carefully to give us matched resolution images ($\sim 0.4''$) at the two frequencies. Fluxes were set using the VLA 1999.2 coefficients for 3C 286. The MERLIN data (5 GHz) was pipeline processed at Jodrell Bank on the Baars et al. (1977) scale, and then combined at Brandeis with a day-long VLA observation recently obtained when the full array was used as a single element for a VSOP space-VLBI experiment. We accounted for variability in the source between the two epochs of observation by subtracting 9.75 Jy from the VLA nucleus in the (u, v) plane. With baselines up to 217 km, this data produced our highest resolution radio image (Figures 1 & 2), which most closely matches that achieved by the *HST* data (~ 0.05 - $0.1''$). Pilbratt, Booth, & Porcas (1987) presented an earlier image of 3C 279 using MERLIN only data. To our knowledge, only the WFPC2 data (Lehnert et al. 1999), but none of the other multi-wavelength observations presented in this work were previously published.

3. ANALYSIS AND RESULTS

The jet emission in the two 1995 FOC exposures appear prominently above the background and wings of the point spread function (PSF). Nevertheless, in order to verify that the extended emission detected was not an artifact of the PSF wings due to the bright nucleus, we subtracted scaled PSFs from each 3C 279 image using images of stars from FOC calibration program ID 6196 (the FOC is insensitive to cosmic rays and a careful inspection of the images did not show any unusual defects near the knot position). The emission from radio knot D clearly remained in the resultant images (not shown). We did not detect any optical counterpart to the rest of the arcsecond-scale jet⁴, where the radio emission is weaker and the radio-to-optical spectrum (based on previous ground based optical imaging) is expected to be steeper: $\alpha_{ro} > 1.1$ (Fraix-Burnet et al. 1991), using the sign convention $F_\nu \propto \nu^{-\alpha}$. Analysis of the radio data and optical limits for the rest of the jet is deferred to a future paper (Marshall et al. 2002b).

We extracted counts from the original (unrotated) geometrically corrected and flat-fielded images using square apertures with 21 pixel ($\sim 0.3''$) sides, centered on the position of the knot (we chose not to extract fluxes from the PSF subtracted images since additional artifacts were introduced from this process). This aperture was judged by eye to contain all the flux from the jet knot, and is situated far enough away from the bright quasar to avoid large contaminations. The background and contribution from the PSF was determined using the same aperture to measure the average count-rates at the three $0.6''$ distant azimuthal positions in 90° intervals around the core. The count

rates were converted to flux densities using the inverse sensitivity measurement given by the PHOTFLAM keyword in the image headers, yielding 6.1 and 1.8 μ Jy at the V and U bands, respectively. We experimented with various circular apertures and found measurement differences on the order of ~ 20 - 25% (higher for the UV data) with that derived above. Therefore, we conservatively estimate this to be the error in our *HST* flux measurements. These fluxes are consistent with (1σ) upper limits of about 10 μ Jy (V) and 6 μ Jy (U) measured from the Poisson noise in the second epoch FOC data.

We used DIFMAP's MODELFIT program to fit elliptical gaussian models to the radio visibility data in the inner region of the jet. The position and size (including ellipticity) derived in this manner for knot D was consistent between the frequencies and gave fluxes of 279 mJy (4.76 GHz) and 115 mJy (15 GHz) which we estimate are accurate to better than 10 and 15%, respectively. The size of the emitting region is best constrained by the MERLIN+VLA image which gives a measured gaussian with dimensions $0.28'' \times 0.06''$, elongated in the jet direction. We estimated a 1.67 GHz flux (650 mJy $\pm 20\%$) from a published MERLIN map (Akujor et al. 1994) of comparable resolution to our new 5 and 15 GHz radio data, giving us a three point *radio* spectral index ($\alpha_r=0.79$) for region D which agrees with the value of 0.75 ± 0.1 measured by de Pater & Perley (1983). The optical and UV fluxes lie below the power-law extrapolation from the radio measurements, indicating steepening at higher frequencies where we measure an optical/UV spectral index of 1.6 with a $2\text{-}\sigma$ confidence of 0.3. The radio-to-UV spectrum is shown in Figure 3.

4. PHYSICAL CONDITIONS IN THE OPTICAL/UV EMITTING REGION

The radio emission from region D shows a high level of fractional polarization (20%) at 5 GHz, but does not appear to be strongly shocked as the magnetic field direction is predominantly longitudinal (de Pater & Perley 1983) indicating a shear dominated flow. Its integrated radio-to-UV spectrum can be well explained by a steepening synchrotron spectrum from a single population of relativistic electrons, as is the usual interpretation for the growing number of already detected optical/UV arcsecond-scale jets (Sparks, Biretta, & Macchetto 1994; Scarpa & Urry 2002). We can extrapolate the radio spectrum to the optical/UV by fitting a break at $\sim 9 \times 10^{13}$ Hz to a smoothly connected double power-law spectrum (Figure 3), so the synchrotron luminosity appears to peak in the near-infrared. If we can extend the observed spectrum to even higher energies, it would predict a 1 keV flux of roughly 0.4 nJy if the X-ray output from the $0.6''$ feature is dominated by synchrotron losses. This should be easily detectable in the *Chandra* exposure obtained by Marshall et al. (2002b), although it may be difficult to resolve with the detector's limited resolution of $0.5''/\text{pixel}$. The measured steepening in the spectral index ($\Delta\alpha \sim 0.8$) corresponds to a change in the electron distribution index Δp (see below) of 1.6. Similar changes have been found for other well-studied high-energy (optical and X-ray) synchrotron emitting regions in the jets of, for instance, M87 (Marshall et al. 2002a) and PKS 0521-365 (Birkinshaw, Worrall, & Hardcastle 2002).

We applied a homogeneous synchrotron model (see e.g., Blumenthal & Gould 1970) to calculate an equipartition magnetic

² The National Radio Astronomy Observatory is a facility of the National Science Foundation operated under cooperative agreement by Associated Universities, Inc.

³ MERLIN is a UK National Facility operated by the University of Manchester at Jodrell Bank Observatory on behalf of PPARC.

⁴ Up to $\sim 3''$ where the field of view of the FOC images was cut off, and for its entire length in the WFPC2 images.

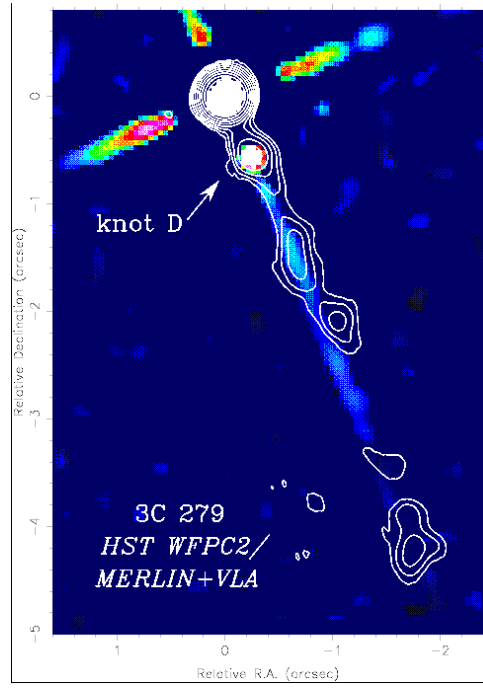


FIG. 2.— *HST* WFPC2 F702W (R-band) image (greyscale plotted logarithmically) with MERLIN+VLA 5 GHz contour image restored with $0.2''$ beam overlaid (see also Figure 1). Optical emission from knot D appears prominently above a diffraction spike after subtraction of a smoothed PSF from the image. The three other diffraction trails extending radially from the nucleus are also apparent. We were unable to identify any optical emission associated with the rest of the radio jet due partly to the unfortunate positioning of the diffraction spike at the position angle of the jet. The radio contours are plotted logarithmically in steps of factor 2 starting at 6 mJy/beam.

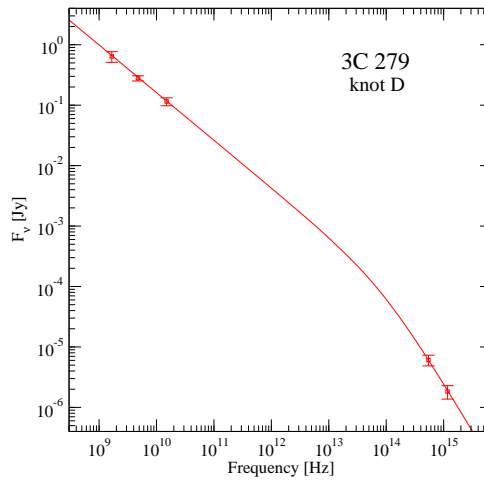


FIG. 3.— The integrated radio-to-UV spectrum of the $\sim 0.6''$ distant region ‘D’ in the kiloparsec scale jet of 3C 279. We fit a smoothly connected double power law spectrum to the data with a break frequency at $\sim 9 \times 10^{13}$ Hz. See text for fluxes and associated errors.

field, $B_{eq} \simeq 1 \times 10^{-3} \times [\eta^{0.26} \gamma_{min}^{-0.15} f^{-0.26} \delta^{-1}] G$. The factor η is defined by the relation: $u_B = \eta u_e$, where u_B and u_e are the energy densities in the magnetic field and electrons, respectively (e.g., if we have equipartition, $\eta = 1$ for an electron-positron plasma). We assumed that the electrons have a power law energy distribution $N(\gamma) \propto \gamma^{-p}$ (with minimum and maximum energy cutoffs, $\gamma_{min} < \gamma < \gamma_{max}$, and $p = 2\alpha + 1$), and that the radiating particles and magnetic field fill a fraction, f , of a spherical volume whose diameter is 4×10^{21} cm (applying an appropriate conversion from our measured elliptical gaussian fit to the size; Marscher (1983)). The Doppler beaming factor is defined as $\delta \equiv [\Gamma(1 - \beta \cos \theta)]^{-1}$, where Γ is the bulk Lorentz factor of the knot, β is the velocity of the jet in units of c , and θ is the angle the jet makes to our line of sight. This calculation is only weakly dependent on γ_{max} which we arbitrarily set to extend into infinity. In the extreme case that the errors in the radio fluxes were even larger than our conservative estimates, it may be possible to obtain a single power law index ($\alpha \sim 1$) fit to the overall radio-to-UV spectrum. Our calculation of B_{eq} in this case maintains relatively unaffected by this steeper spectral index. The derived magnetic field implies that the UV emitting electrons have $\gamma \simeq 8 \times 10^5 \times [\eta^{-0.13} \gamma_{min}^{0.08} f^{0.13}]$ with a radiative lifetime (in their rest frame) of about $20 \times [\eta^{-0.39} \gamma_{min}^{0.22} f^{0.39} \delta^2]$ yrs.

It is useful to see how the synchrotron cooling time of the UV emitting electrons in knot D compares with the light travel distance from the nucleus. Firstly, the angle between the jet and our line of sight is restricted to be $\leq 8^\circ$ by the observed VLBI apparent superluminal motion of 14c (Cotton et al. 1979). We

note that this measurement is the fastest (and earliest) motion recorded in this quasar so far, and was observed when the VLBI jet was best aligned ($218^\circ \pm 2^\circ$) with the position angle of the VLA scale jet ($\sim 205^\circ$). This gives us a deprojected distance from the nucleus to knot D of $\gtrsim 25$ kpc. Now, if the Doppler factor this far down the jet is as large as that observed on parsec-scales ($\delta = 20$; Homan & Wardle 2000), and making the simple assumptions, $\eta = 1$, $\gamma_{min} = 10$, and $f = 1$, we can infer a rest-frame $B_{eq} \sim 4 \times 10^{-5}$ G – comparable to those derived for other known optical emitting synchrotron features (see e.g., Scarpa & Urry 2002). It follows that the *observed* (accounting for time dilation between the rest frame and observer frame) radiative lifetime is $\sim 3 \times 10^5$ yrs which corresponds to a travel distance of ~ 90 kpc and exceeds the light travel time from the nucleus by a factor of a few. This makes it just plausible that *in-situ* reacceleration (e.g., Meisenheimer 1996) is not strictly required if the Doppler factor at the site of knot D is really as high as that measured on parsec scales, but that remains unknown.

The author is grateful to John Wardle for a careful reading of the manuscript and continued support of his research, to Herman Marshall for communications which inspired the *HST* archive search and support of this work, and to Dave Roberts, Dan Homan, Niruj Mohan, Fabrizio Tavecchio, Robert Jedrzejewski, and Andy McDonald for invaluable discussions. Radio astronomy at Brandeis University is supported by the National Science Foundation through grants AST 98-02708 and AST 99-00723.

REFERENCES

- Akujor, C. E., Lüdke, E., Browne, I. W. A., Leahy, J. P., Garrington, S. T., Jackson, N., & Thomasson, P. 1994, A&AS, 105, 247
 Attridge, J. M. 2001, ApJ, 553, L31
 Baars, J. W. M., Genzel, R., Pauliny-Toth, I. I. K., & Witzel, A. 1977, A&A, 61, 99
 Birkinshaw, M., Worrall, D. M., & Hardcastle, M. J. 2002, MNRAS, 335, 142
 Blumenthal, G. R. & Gould, R. J. 1970, Rev. Mod. Phys., 42, 237
 Cotton, W. D. et al. 1979, ApJ, 229, L115
 de Pater, I. & Perley, R. A. 1983, ApJ, 273, 64
 Fraix-Burnet, D., Golombek, D., Macchetto, F., Nieto, J.-L., Lelievre, G., Perryman, M. A. C., & di Serego Alighieri, S. 1991, AJ, 101, 88
 Greisen, E. W. 1988, AIPS Memo 61, National Radio Astronomy Observatory
 Hartman, R. C., Boettcher, M., Aldering, G. et al. 2001, ApJ, 553, 683
 Homan, D. C. & Wardle, J. F. C. 1999, AJ, 118, 1942
 —. 2000, ApJ, 535, 575
 Hook, R. N., Schreier, E. J., & Miley, G. 2000, ApJ, 536, 308
 Jedrzejewski, R. I., Hartig, G., Jakobsen, P., Crocker, J. H., & Ford, H. C. 1994, ApJ, 435, L7
 Lehnert, M. D., Miley, G. K., Sparks, W. B., Baum, S. A., Biretta, J., Golombek, D., de Koff, S., Macchetto, F. D., & McCarthy, P. J. 1999, ApJS, 123, 351
 Leppänen, K. J., Zensus, J. A., & Diamond, P. J. 1995, AJ, 110, 2479
 Marscher, A. P. 1983, ApJ, 264, 296
 Marshall, H. L., Miller, B. P., Davis, D. S., Perlman, E. S., Wise, M., Canizares, C. R., & Harris, D. E. 2002a, ApJ, 564, 683
 Marshall, H. L. et al. 2002b, in preparation
 Meisenheimer, K. 1996, In "Jets from Stars and Active Galactic Nuclei," W. Kundt (ed.), Springer Lecture Notes No. 471, 57
 Pilbratt, G., Booth, R. S., & Porcas, R. W. 1987, A&A, 173, 12
 Scarpa, R. & Urry, C. M. 2002, New Astronomy Review, 46, 405
 Shepherd, M. C., Pearson, T. J., & Taylor, G. B. 1994, BAAS, 26, 987
 Sparks, W. B., Biretta, J. A., & Macchetto, F. 1994, ApJS, 90, 909
 Thompson, A. R., Clark, B. G., Wade, C. M., & Napier, P. J. 1980, ApJS, 44, 151
 Unwin, S. C., Cohen, M. H., Hodges, M. W., Zensus, J. A., & Biretta, J. A. 1989, ApJ, 340, 117
 Wardle, J. F. C., Homan, D. C., Ojha, R., & Roberts, D. H. 1998, Nature, 395, 457
 Wehrle, A. E., Pian, E., Urry, C. M. et al. 1998, ApJ, 497, 178
 Wehrle, A. E., Piner, B. G., Unwin, S. C., Zook, A. C., Xu, W., Marscher, A. P., Teräsranta, H., & Valtaoja, E. 2001, ApJS, 133, 297

TABLE 1
SUMMARY OF ARCHIVAL OBSERVATIONS

Instrument (1)	Date (2)	Frequency (3)	Exp Time (4)
MERLIN	04 Jan 1993	4.99	~9 hrs
VLA A-configuration	10 Jan 2001	4.87	~7 hrs
VLA A-configuration	12 Mar 1990	4.76	580 sec
VLA B-configuration	06 Jan 1992	15.0	2690 sec
<i>HST</i> WFPC2/F702W	23 Feb 1994	4.33×10^5	300 sec
<i>HST</i> WFPC2/F702W	20 May 1995	4.33×10^5	300 sec
<i>HST</i> FOC/F550M	29 Nov 1995	5.44×10^5	1115 sec
<i>HST</i> FOC/F253M	29 Nov 1995	1.17×10^6	935 sec

Note. — Column (1) indicates the telescope and instrument/configuration used. The MERLIN observations utilized a six element array (no Lovell). The WFPC2 data was not used for photometric analysis.

Column (2) is the date of observation in UT.

Column (3) is the frequency in GHz.

Column (4) is the time on source with approximate times indicated for heavily edited data.